Rapidly prototyping kagome flat band physics with acoustic metamaterials

Jiatong Yang,[1,2,3] Benjamin H. November,[2] Yiting Huang,[2,4]
S. Minhal Gardezi,[1,5] Harris Pirie,[2,6] and Jennifer E. Hoffman[2,5,*]

[1]*Department of Physics, Wellesley College, Wellesley MA, 02481, USA*
[2]*Department of Physics, Harvard University, Cambridge, MA 02138, USA*
[3]*Department of Physics, Massachusetts Institute of Technology, Cambridge, MA, 02139, USA*
[4]*Department of Physics, Stanford University, Stanford, CA 94305, USA*
[5]*School of Engineering & Applied Sciences, Harvard University, Cambridge, MA 02138, USA*
[6]*Department of Materials Science and NanoEngineering, Rice University, Houston, TX, 77005, USA*

(Dated: July 8, 2026)

Flat bands with vanishing group velocity and quenched kinetic energy provide fertile ground for correlated states and exotic phenomena such as unconventional superconductivity. Yet, engineering and characterizing flat bands in quantum materials is time-consuming and costly, limiting the exploration of the vast design space of possible flat band systems. Acoustic metamaterials offer an accessible alternative: they can be easily simulated, cheaply fabricated, and quickly measured. Here we present a complete workflow to rapidly prototype flat band systems using acoustic metamaterials. Our design directly implements a tight-binding model using air cavities as lattice sites connected by channels that control hopping, allowing it to generalize to diverse lattice geometries. Using the kagome lattice as a proof-of-concept, we demonstrate excellent agreement between tight-binding theory, finite-element simulations, and experimental measurements. We then design a family of extended kagome lattices whose added sites cancel successively longer-range hopping, flattening the flat band. With fabrication and measurement requiring hours rather than months and a total cost orders of magnitude lower than quantum materials, our approach enables rapid iteration through candidate lattices, facilitating the discovery of new flat band physics in quantum materials.

1 Electronic flat bands provide a rich platform for novel quantum phases due to their low kinetic energy and high degeneracy. Their low group velocity emphasizes the role of electron interactions, which would usually be dwarfed by the kinetic energy of dispersive bands. Such strong interactions underpin phenomena such as magnetism and Kondo effects [1], fractionalization [2], and strange metals and hydrodynamic flow [3]. Degeneracy enables the highly-entangled many-body states required for topological quantum computing [4]. Flat bands can promote superconductivity both by concentrating many states near the Fermi level for pairing and by increasing the relative importance of pairing interactions compared with kinetic energy [5, 6], while the quantum geometry of the flat band can provide finite superfluid stiffness despite the vanishing conventional band-velocity contribution [7]. Recent experiments show rapid developments in flat band physics [8], such as the correlated insulating phase and unconventional superconductivity in magic-angle twisted bilayer graphene [9], as well as exotic properties in kagome lattices [10–14]. The search is now expanding towards materials with even flatter bands and different symmetry representations [15]. However, the synthesis, characterization, and optimization of each candidate quantum material among the vast phase space of possibilities is time-consuming and costly.

2 To address these challenges, other flexible platforms have been employed to study flat band systems, including cold atoms trapped in optical lattices [16–19], photonic metamaterials [20–22], mechanical metamaterials [23–25], and acoustic metamaterials [26–44]. Among these, acoustic metamaterials are especially well suited for a rapid prototyping workflow as they can be simulated in minutes, fabricated at modest cost, and measured in hours. Within the past decade, acoustic metamaterials have reproduced many apparently quantum effects, including quantum Hall phases in graphene [26, 27], topological phases with quantized multiple moments [28–30], and topological semimetals [31, 32]. More recently, acoustic flat bands have been realized and studied in twisted moiré lattices [33–36], Landau level systems [27, 37–39], kagome lattices [40, 41], and others [42–44]. These studies establish the feasibility of creating and measuring acoustic flat bands, and initial workflows that connect simulation, fabrication, and experiment are beginning to emerge. However, to fully unlock the potential of acoustic platforms as a general-purpose tool for flat-band prototyping, more systematic and broadly accessible design-to-experiment workflows are needed.

3 Here, we present a complete workflow for rapidly prototyping flat band lattices with acoustic metamaterials. We demonstrate each step using the kagome lattice as a proof-of-concept. Starting from the tight-binding Hamiltonian, we design an analogous acoustic metamaterial where air cavities act as lattice sites, and connecting channels control the hopping strength between them. We use COMSOL Multiphysics to optimize the design parameters and predict the acoustic band structure. We then CNC-mill the metamaterial from aluminum, though the design principles apply to any other fabrication method and material with sufficient acoustic

* jhoffman@g.harvard.edu

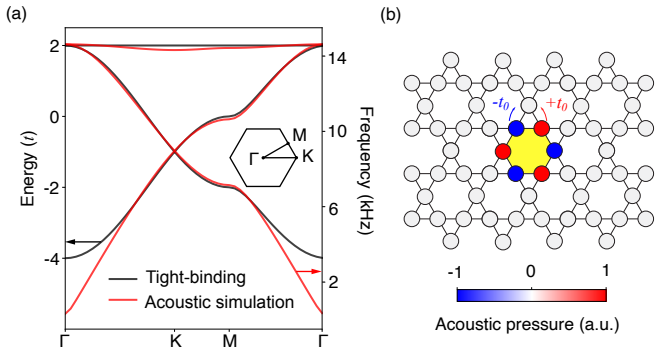


FIG. 1. Kagome lattices host a geometric flat band. (a) Tight-binding (black) and COMSOL-computed acoustic (red) band structures of the kagome lattice show good agreement. Both feature two dispersive bands forming a Dirac cone at the K point, and a flat band that touches them at the Γ point. (b) The flat band arises from destructive interference between sites of opposite phase (blue and red), which cancels hopping to neighboring sites and confines the mode to a single hexagonal plaquette (yellow).

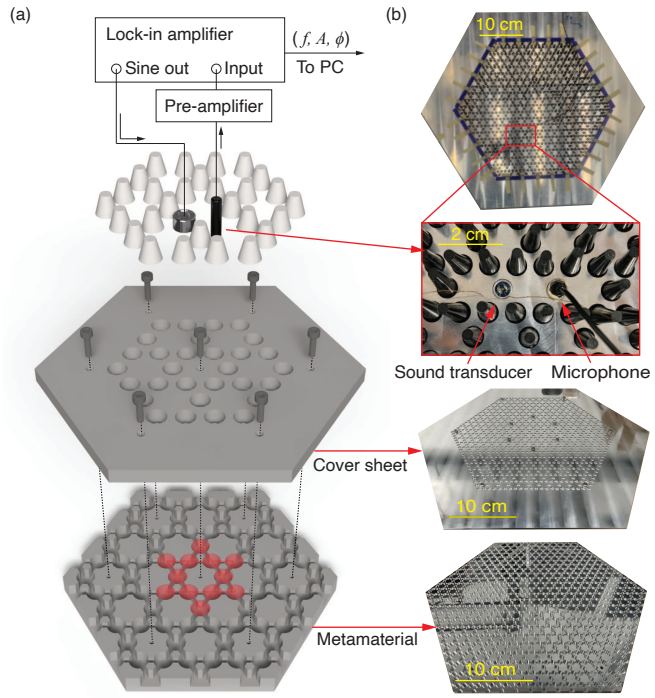


FIG. 2. Experimental apparatus to measure acoustic flat bands (a) A lock-in amplifier generates a sinusoidal drive signal for the sound transducer and performs phase-sensitive detection of the microphone signal via a pre-amplifier. The metamaterial consists of a total of 1296 cavities arranged in a kagome lattice (highlighted in red) enclosed by a removable cover sheet. (b) Photographs of the fabricated acoustic kagome metamaterial.

impedance contrast. Using a simple experimental setup, we measure the acoustic response at each lattice site, and directly visualize both the compact localized states in real space and the complete band structure in momentum space. Our experimental results show good agreement with both tight-binding theory and COMSOL simulations, demonstrating a practical platform for exploring flat band physics.

4 The kagome lattice is a canonical example that hosts a geometrically-protected flat band. In a tight-binding model with only nearest-neighbor hopping, it contains two dispersive bands forming Dirac cones at the K and K' points of the Brillouin zone, and a perfectly flat band that touches them at the Γ point (Fig. 1(a)). This flat band originates from the destructive interference between hopping terms: its real-space mode has equal amplitude but alternating sign on the six sites of the hexagon, so that hopping to neighboring sites interfere destructively and the wave function remains confined to a single hexagonal plaquette (Fig. 1(b)). The result is a compact localized state with zero group velocity—the defining characteristic of a perfectly flat band. In a more realistic model, next-nearest-neighbor hopping introduces a slight dispersion, but the group velocity remains near zero.

5 We designed an acoustic metamaterial that directly implements the kagome tight-binding model. In our system, an array of air cavities hold acoustic modes analogous to atomic orbitals, while interconnecting air channels control the nearest-neighbor hopping t_0 between sites. We focus on the lowest-frequency cavity modes, which exhibit nearly uniform pressure and are analogous to atomic s orbitals. The cavities and channels are cut into a solid lattice layer and sealed within boundary sheets to contain the acoustic pressure. Because the acoustic impedance of the solid exceeds that of air by more than two orders of magnitude, sound waves propagate almost entirely through the engineered air lattice, with negligible leakage into the surrounding solid. This impedance confinement ensures that the acoustic band structure is determined solely by the tight-binding geometry, rather than material choice. Our design allows straightforward implementation and tuning of diverse lattice geometries using either subtractive (cutting, milling) or additive (3D printing) fabrication techniques.

6 We quantified our design using finite-element simulations with COMSOL Multiphysics. Our kagome metamaterial is composed of a 5-mm-thick aluminum slab with cavity radius 3.5 mm, channel width 2 mm, and nearest-neighbor distance 8.66 mm. We calculated the acoustic band structure by solving for the eigenfrequencies along a high-symmetry path in reciprocal space under Floquet-periodic boundary conditions. A complete COMSOL simulation with 48 k-points required only 85 seconds, demonstrating the computational efficiency of the acoustic model. The resulting band structure reproduces the kagome lattice's Dirac cone and flat band, in good agreement with the tight-binding model despite the realistic inclusion of longer-range hopping in the simulation (see comparison in Fig. 1(a)). From this fit, we extracted the effective nearest-neighbor hopping amplitude

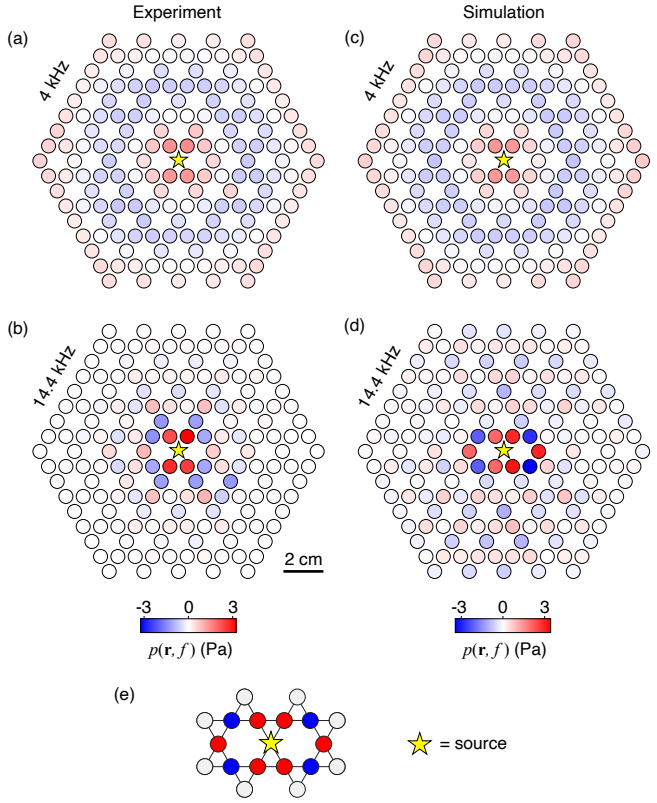


FIG. 3. Real-space mapping of dispersive and localized modes in the acoustic kagome lattice. (a)-(b) Experimental measurements of the acoustic field at 4 kHz (dispersive mode) and 14.4 kHz (flat-band mode). The star marks the position of the sound transducer. At 4 kHz, the excitation propagates across the lattice, while at 14.4 kHz the response is strongly confined around the source, demonstrating flat-band localization. (c)-(d) COMSOL simulations of the corresponding modes show excellent agreement with experiment. We emphasize that the identical quantitative color scale for pressure is used for all measurements and calculations shown here in (a)-(d). (e) Schematic of the compact localized state expected from a single central source.

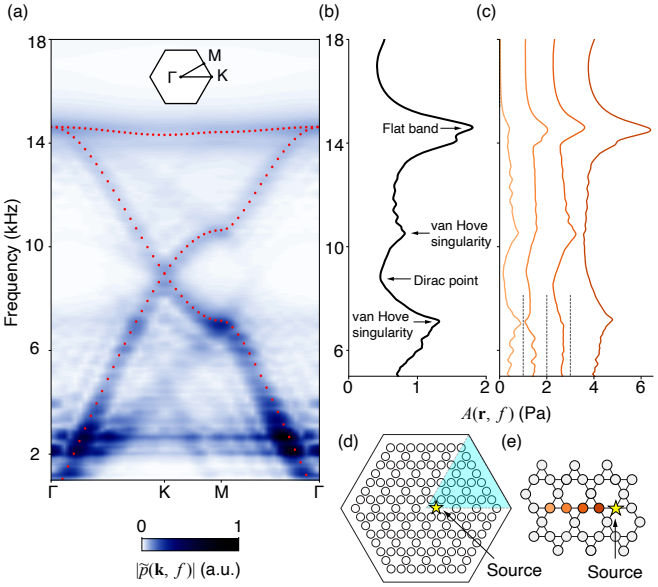


FIG. 4. Spectroscopic evidence of a localized flat band in an acoustic kagome metamaterial. (a) The experimentally reconstructed band structure (blue colorscale) obtained from the spatial Fourier transform of the measured pressure fields matches the simulated band structure (red points). There are several less prominent bands that arise from the boundary effects in the finite-size Fourier transform. The inset shows a schematic of the Brillouin zone sweep. (b) The averaged sound-pressure spectrum from the 14 cavities nearest the source exhibits the characteristic features of a kagome lattice: a dip at the Dirac point, peaks at the two Van Hove singularities, and a pronounced resonance at the flat-band frequency. (c) Individual cavity spectra show that the flat-band resonance decays rapidly with distance from the source, while the dispersive modes maintain similar amplitudes across the lattice, confirming the localized nature of the flat-band state. The spectra have shifted origins (marked with dashed lines) along the horizontal axis for clarity. (d) Schematic of the kagome metamaterial (not drawn to scale and doesn't include all cavities). The cyan shading shows the cavities where the band structure data in (a) were obtained. (e) Color-coded schematic of the cavities in which the response curves in (c) were acquired.

$t_0 = 1.75$ kHz.

7 We designed an experimental apparatus for accessible, efficient, and precise acoustic mapping in both real and momentum space (Fig. 2). The kagome lattice and bottom boundary layer were CNC-machined from a single piece of aluminum and sealed with a removable cover plate. The cover contains an array of small access holes above each cavity, allowing us to excite acoustic modes with a sound transducer in one cavity and measure the response by scanning a microphone across all other sites. Unused holes are sealed with rubber plugs. We use a lock-in amplifier both to generate a monofrequency transducer tone and to enable phase-sensitive detection at each cavity location $\mathbf{r_i}$: the microphone output is amplified then returned to the lock-in to extract the amplitude $A(\mathbf{r_i}, f)$ and phase $\phi(\mathbf{r_i}, f)$ at the driving frequency f. The steady-state acoustic wave function can be reconstructed by calculating the time-dependent pressure

$$p(\mathbf{r_i}, f, t) = A(\mathbf{r_i}, f)e^{-i(2\pi f t + \phi(\mathbf{r_i}, f))}. \quad (1)$$

Typically, we focus on the time-independent solutions

$$p(\mathbf{r_i}, f) = A(\mathbf{r_i}, f)e^{-i\phi(\mathbf{r_i}, f)}. \quad (2)$$

We compute the complete two-dimensional band structure from the Fourier transform of $p(\mathbf{r_i}, f)$

$$\tilde{p}_n(\mathbf{k}, f) = \sum_i A(\mathbf{r_i}, f)e^{-i\phi(\mathbf{r_i}, f)}e^{-i\mathbf{k}\cdot\mathbf{r_i}}, \quad (3)$$

where i is summing over all cavities in the sublattice n. Then we sum over all three kagome sublattices to obtain

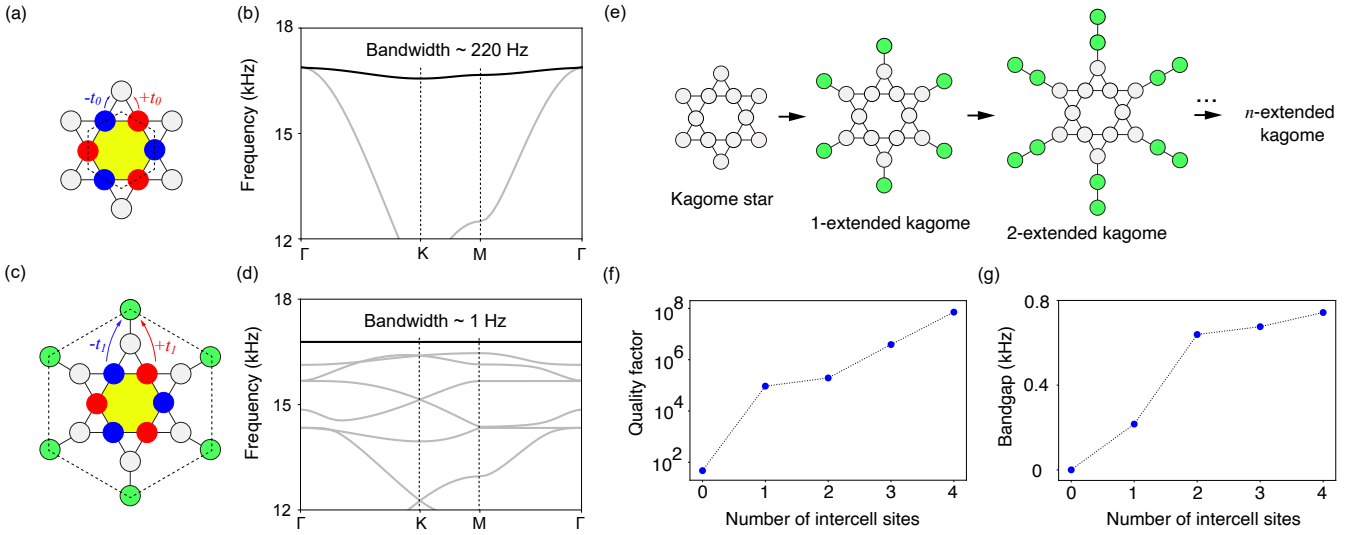


FIG. 5. Extended kagome hosts an isolated, ultra-flat band. (a) Unit cell of the kagome lattice and (b) COMSOL simulation shows flat band quality factor $Q \sim 76$ (bandwidth / band energy). (c) Unit cell of extended kagome. Note that the green sites cancel the next-nearest-neighbor hopping t_1 from the red and blue sites, thus further localizing the mode to the yellow region. (d) COMSOL-simulated band structure of extended kagome. The top band is unpinned from the rest of the dispersive bands and is flatter than the kagome flat band, with $Q \sim 13,700$. (e) The unit cell of n-extended kagome is constructed by adding n cavities (green) to the kagome star. (f) The quality factor of the flat band increases almost exponentially with the number of intercell sites. (g) The energy gap between the flat and dispersive bands increases with the number of intercell sites added.

the average Fourier amplitude

$$|\tilde{p}(\mathbf{k}, f)| = \frac{1}{3} \sum_n |\tilde{p}_n(\mathbf{k}, f)|. \tag{4}$$

Measuring a single cavity with high signal-to-noise takes approximately 0.5 seconds per frequency point. Including manual microphone repositioning, measuring a 100–200 cavity lattice over its entire bandwidth requires 4–8 hours.

8 Our apparatus can directly image real-space acoustic wave functions, making it straightforward to distinguish between the propagating modes of dispersive bands and the localized states of a flat band. We first excited the lattice at a frequency of 4 kHz, within the lower dispersive band. This excitation induced a propagating wave spreading from the transducer to fill the entire lattice (Fig. 3(a) and supplementary video in Appendix A). In contrast, at the flat-band frequency of 14.4 kHz, the response remained tightly confined near the source and decayed rapidly beyond the first unit cell (Fig. 3(b)). This rapid decay is a consequence of destructive interference in the kagome lattice, which we directly observed through the alternating phases between neighboring sites. The overall response can be understood as a superposition of two compact localized states of the form shown in Fig. 1(a), as highlighted schematically in Fig. 3(e). The localized flat-band state reached a higher peak pressure amplitude than the dispersive bands—a consequence of concentrating the acoustic energy in a confined region. Our experimental measurements are in agreement with the finite-element simulations for both the propagating mode (Fig. 3(c)) and the confined flat-band mode (Fig. 3(d)).

9 To complete our characterization, we reconstructed the full acoustic band structure in Fig. 4 by calculating the average Fourier amplitude shown in Eq. (4). To achieve high k-space resolution of around 0.4 cm^{-1} within a reasonable measurement time, we sampled a triangular region containing one-sixth of the lattice sites (Fig. 4(d)). Then we symmetrized the Fourier-transformed data from Eq. (4) to recover the sixfold rotational symmetry of the Brillouin zone. In total, we measured 185 cavities in around 8 hours, though this process could be substantially accelerated using a multiplexed or automated scanning system. The resulting experimental band structure agrees with both the finite-element simulations and tight-binding calculations, displaying a clear Dirac cone at the K point and a high-intensity flat band at around 14.4 kHz (Fig. 4(a)). Averaging the amplitude over the 14 cavities nearest to the source provides an estimate of the local density of states, revealing the characteristic kagome-lattice features: a dip at the Dirac point, two van Hove peaks, and a dominant flat band maximum (Fig. 4(b)). Single-site spectra recorded at increasing distances from the source confirm the localized nature of the flat band, as its spectral peak decays much faster than those of the propagating modes (Fig. 4(c)).

10 Our rapid prototyping workflow can be used not only to study existing flat band systems, but also to explore lattices that do not exist naturally. As a demonstration, we designed a family of extended kagome lattices whose flat bands become progressively flatter. In

the conventional kagome lattice, next-nearest neighbor hopping t_1 prevents a perfectly flat band (Fig. 5(a,b)). Our extended kagome lattice adds one site outside each kagome star, so that both the nearest-neighbor hopping t_0 and the next-nearest-neighbor hopping t_1 interfere destructively (Fig. 5(c)). The extended kagome flat band is more than two orders of magnitude flatter than the kagome flat band, and is also unpinned from the rest of the dispersive bands (Fig. 5(d)). Adding n sites in between the kagome stars cancels the hopping terms up to t_n, creating a series of "n-extended kagome" lattices with progressively flatter bands (Fig. 5(e)). Using COMSOL to simulate the first four lattices in the series, we found that both flat band quality factor and energy gap increase with n (Fig. 5(f,g)). The flat-band quality factor increases nearly exponentially with n, as expected because each additional intercell site increases the effective separation between neighboring kagome units and thus exponentially suppresses the hopping t that sets the residual bandwidth.

11 Our work establishes a practical bridge between theoretical flat-band models and experimental realization, transforming studies from months-long materials synthesis to hours-long table-top experiments. By directly imaging both the real-space acoustic wave functions and the full momentum-space acoustic band structure, we simultaneously captured the compact localized states and near zero group velocity of the kagome lattice – features that underpin correlation, topology, and superconductivity in electronic systems. Beyond the simple kagome lattice, our framework offers a route to experimentally explore the vast phase space of flat-band systems, including large moiré geometries where conventional theoretical and numerical approaches reach their limits [45] and artificially designed lattices that do not yet exist in nature such as the "n-extended kagome" lattice.

[1] L. Kouwenhoven and L. Glazman, Revival of the Kondo effect, Physics World **14**, 33 (2001).

[2] T. Senthil and M. P. A. Fisher, z_2 gauge theory of electron fractionalization in strongly correlated systems, Physical Review B **62**, 7850 (2000).

[3] A. Lucas and S. A. Hartnoll, Resistivity bound for hydrodynamic bad metals, Proceedings of the National Academy of Sciences **114**, 11344 (2017).

[4] C. Nayak, S. Simon, A. Stern, M. Freedman, and S. Das Sarma, Non-abelian anyons and topological quantum computation, Reviews of Modern Physics **80**, 1083 (2008).

[5] J. Bardeen, L. N. Cooper, and J. R. Schrieffer, Theory of superconductivity, Physical Review **108**, 1175 (1957).

[6] N. B. Kopnin, T. T. Heikkilä, and G. E. Volovik, High-temperature surface superconductivity in topological flat-band systems, Physical Review B **83**, 220503 (2011).

[7] A. Julku, S. Peotta, T. I. Vanhala, D.-H. Kim, and P. Törmä, Geometric origin of superfluidity in the Lieb-lattice flat band, Physical Review Letters **117**, 045303 (2016).

[8] J. G. Checkelsky, B. A. Bernevig, P. Coleman, Q. Si, and S. Paschen, Flat bands, strange metals and the Kondo effect, Nature Reviews Materials **9**, 509 (2024).

[9] Y. Cao, V. Fatemi, S. Fang, K. Watanabe, T. Taniguchi, E. Kaxiras, and P. Jarillo-Herrero, Unconventional superconductivity in magic-angle graphene superlattices, Nature **556**, 43 (2018).

[10] E. Tang, J.-W. Mei, and X.-G. Wen, High-temperature fractional quantum Hall states, Physical Review Letters **106**, 236802 (2011).

[11] T. Neupert, L. Santos, C. Chamon, and C. Mudry, Fractional quantum Hall states at zero magnetic field, Physical Review Letters **106**, 236804 (2011).

[12] K. Sun, Z. Gu, H. Katsura, and S. Das Sarma, Nearly flatbands with nontrivial topology, Physical Review Letters **106**, 236803 (2011).

[13] W. Zhu, S.-S. Gong, T.-S. Zeng, L. Fu, and D. N. Sheng, Interaction-driven spontaneous quantum Hall effect on a kagome lattice, Physical Review Letters **117**, 096402 (2016).

[14] L. Ye, S. Fang, M. Kang, J. Kaufmann, Y. Lee, C. John, P. M. Neves, S. Y. F. Zhao, J. Denlinger, C. Jozwiak, A. Bostwick, E. Rotenberg, E. Kaxiras, D. C. Bell, O. Janson, R. Comin, and J. G. Checkelsky, Hopping frustration-induced flat band and strange metallicity in a kagome metal, Nature Physics **20**, 610 (2024).

[15] L. Chen, F. Xie, S. Sur, H. Hu, S. Paschen, J. Cano, and Q. Si, Emergent flat band and topological Kondo semimetal driven by orbital-selective correlations, Nature Communications **15**, 5242 (2024).

[16] G.-B. Jo, J. Guzman, C. K. Thomas, P. Hosur, A. Vishwanath, and D. M. Stamper-Kurn, Ultracold atoms in a tunable optical kagome lattice, Physical Review Letters **108**, 045305 (2012).

[17] S. Taie, H. Ozawa, T. Ichinose, T. Nishio, S. Nakajima, and Y. Takahashi, Coherent driving and freezing of bosonic matter wave in an optical Lieb lattice, Science Advances **1**, e1500854 (2015).

[18] H. Ozawa, S. Taie, T. Ichinose, and Y. Takahashi, Interaction-driven shift and distortion of a flat band in an optical Lieb lattice, Physical Review Letters **118**, 175301 (2017).

[19] S. Taie, T. Ichinose, H. Ozawa, and Y. Takahashi, Spatial adiabatic passage of massive quantum particles in an optical Lieb lattice, Nature Communications **11**, 257 (2020).

[20] Y. Nakata, T. Okada, T. Nakanishi, and M. Kitano, Observation of flat band for terahertz spoof plasmons in a metallic kagomé lattice, Physical Review B **85**, 205128 (2012).

[21] F. Baboux, L. Ge, T. Jacqmin, M. Biondi, E. Galopin, A. Lemaître, L. Le Gratiet, I. Sagnes, S. Schmidt, H. E. Türeci, A. Amo, and J. Bloch, Bosonic condensation and disorder-induced localization in a flat band, Physical Review Letters **116**, 066402 (2016).

[22] Y. Zong, S. Xia, L. Tang, D. Song, Y. Hu, Y. Pei, J. Su,

Y. Li, and Z. Chen, Observation of localized flat-band states in Kagome photonic lattices, Optics Express **24**, 8877 (2016).
[23] M. Rosendo López, F. Peñaranda, J. Christensen, and P. San-Jose, Flat bands in magic-angle vibrating plates, Physical Review Letters **125**, 214301 (2020).
[24] P. Karki and J. Paulose, Non-singular and singular flat bands in tunable phononic metamaterials, Physical Review Research **5**, 023036 (2023).
[25] M. M. Samak and O. R. Bilal, Direct observation of all-flat bands phononic metamaterials, Physical Review Letters **133**, 266101 (2024).
[26] Y. Ding, Y. Peng, Y. Zhu, X. Fan, J. Yang, B. Liang, X. Zhu, X. Wan, and J. Cheng, Experimental demonstration of acoustic Chern insulators, Physical Review Letters **122**, 014302 (2019).
[27] X. Wen, C. Qiu, Y. Qi, L. Ye, M. Ke, F. Zhang, and Z. Liu, Acoustic Landau quantization and quantum-Hall-like edge states, Nature Physics **15**, 352 (2019).
[28] M. Xiao, G. Ma, Z. Yang, P. Sheng, Z. Q. Zhang, and C. T. Chan, Geometric phase and band inversion in periodic acoustic systems, Nature Physics **11**, 240 (2015).
[29] H. Xue, Y. Yang, F. Gao, Y. Chong, and B. Zhang, Acoustic higher-order topological insulator on a kagome lattice, Nature Materials **18**, 108 (2019).
[30] Y. Qi, C. Qiu, M. Xiao, H. He, M. Ke, and Z. Liu, Acoustic realization of quadrupole topological insulators, Physical Review Letters **124**, 206601 (2020).
[31] M. Xiao, W.-J. Chen, W.-Y. He, and C. T. Chan, Synthetic gauge flux and Weyl points in acoustic systems, Nature Physics **11**, 920 (2015).
[32] F. Li, X. Huang, J. Lu, J. Ma, and Z. Liu, Weyl points and Fermi arcs in a chiral phononic crystal, Nature Physics **14**, 30 (2018).
[33] S. M. Gardezi, H. Pirie, S. Carr, W. Dorrell, and J. E. Hoffman, Simulating twistronics in acoustic metamaterials, 2D Materials **8**, 031002 (2021).
[34] C. Han, S. Fan, H.-T. Zhou, K. He, Y. Jia, C. Li, H. Li, X.-D. Yang, L.-Q. Chen, T. Yang, and C.-W. Qiu, All-angle unidirectional flat-band acoustic metasurfaces, Nature Communications **16**, 634 (2025).
[35] X. Zhang, T. Liu, Q. Zhang, X. Fan, F. Wu, and C. Qiu, Observation of ultraflat bands in gapped moiré metamaterials, Physical Review B **111**, 125143 (2025).
[36] S. Fan, C. Han, K. He, L. Bai, L. Chen, H. Shi, C. Shen, and T. Yang, Acoustic moiré flat bands in twisted heterobilayer metasurface, Advanced Materials **37**, 2418839 (2025).
[37] Z. Cheng, Y.-J. Guan, H. Xue, Y. Ge, D. Jia, Y. Long, S.-Q. Yuan, H.-X. Sun, Y. Chong, and B. Zhang, Three-dimensional flat Landau levels in an inhomogeneous acoustic crystal, Nature Communications **15**, 2174 (2024).
[38] P. Li, W. Chen, J. Chen, W. Luo, and D. Zhao, Acoustic Landau levels in a synthetic magnetic field with a symmetric gauge, Physical Review Applied **22**, 014047 (2024).
[39] Q. Mo, R. Zheng, C. Lu, X. Huang, Z. Liu, and S. Zhang, Observation of oriented Landau levels and helical zero modes in Berry dipole acoustic crystals, Physical Review Letters **134**, 116604 (2025).
[40] B. Jiang, A. Bouhon, Z.-K. Lin, X. Zhou, B. Hou, F. Li, R.-J. Slager, and J.-H. Jiang, Experimental observation of non-Abelian topological acoustic semimetals and their phase transitions, Nature Physics **17**, 1239 (2021).
[41] E. Riva, F. Bellinzoni, and F. Braghin, Creating compact localized modes for robust sound transport via singular flat band engineering, Communications Physics **8**, 255 (2025).
[42] X. Shi and J. Yang, Spin-1 Weyl point and surface arc state in a chiral phononic crystal, Physical Review B **101**, 214309 (2020).
[43] Y.-X. Shen, Y.-G. Peng, P.-C. Cao, J. Li, and X.-F. Zhu, Observing localization and delocalization of the flat-band states in an acoustic cubic lattice, Physical Review B **105**, 104102 (2022).
[44] W. Zhu, H.-y. Zou, Y. Ge, Y. Wang, Z. Cheng, B.-b. Wang, S.-q. Yuan, H.-x. Sun, H. Xue, and B. Zhang, Flatbands from bound states in the continuum for orbital angular momentum localization, Nature Communications **17**, 3065 (2026).
[45] S. Carr, S. Fang, and E. Kaxiras, Electronic-structure methods for twisted moiré layers, Nature Reviews Materials **5**, 748 (2020).

Appendix A: Time evolution

Our apparatus can directly image real-space acoustic wave functions. In addition to the snapshots presented in Fig. 4 of the main text, we include a video showing the time evolution of excitations within the dispersive regime (4 kHz) and the flat band regime (14.4 kHz). At 4 kHz, the transducer induced a propagating wave spreading from the center to fill the entire lattice, whereas at the flat-band frequency of 14.4 kHz, the response remained tightly confined near the source and decayed rapidly beyond the first unit cell. Measured acoustic pressure and COMSOL simulation show excellent agreement in both frequency regimes.

https://hoffman.physics.harvard.edu/publications/Yang-metamaterial-kagome-flat-band.gif

Appendix B: Cost table

The total equipment cost for our setup was about $5,700, with the lock-in amplifier representing the bulk of the expense (see Table I for detailed cost breakdown). These equipments can be reused for measuring other metamaterials, so the cost per experiment can be reduced. The aluminum kagome lattice cost approximately $1,750 to fabricate. This could be reduced with 3D printing at the expense of lower acoustic impedance and reduced quality factor, which may still be acceptable for some applications [27, 35]. Overall, the total cost of our approach is orders of magnitude lower than synthesizing and characterizing quantum materials, which can easily reach tens of thousands of dollars when considering equipment, materials, and labor.

Product	**Part No. / Description**	**Qty.**	**Unit Price (USD)**	**Total (USD)**
Transducer	Knowles SR6438NWS-000	1	7.66	7.66
Microphone	DPA 6060-OC-U-B00	1	640.00	640.00
Microlock to XLR adapter	DPA DAD9001	1	125.00	125.00
Microphone preamplifier	M-Audio DMP3	1	100.00	100.00
Lock-in amplifier	Stanford Research SR830	1	4,795.00	4,795.00
			Measurement setup total:	**5,667.66**
Silicone plugs	STP102	1,300	0.0417	54.21
Lattice layer (CNC machined)	Aluminum	1	1,005.52	1,005.52
Cover sheet (CNC machined)	Aluminum	1	676.67	676.67
			Metamaterial total:	**1,736.40**

TABLE I. Breakdown of material and setup costs. The measurement setup includes reusable instruments, dominated by the cost of the lock-in amplifier. The metamaterial costs include components specific to prototyping a single lattice.